International Journal of Solids and Structures 48 (2011) 2605–2613

Contents lists available at ScienceDirect

International Journal of Solids and Structures

journal homepage: www.elsevier.com/locate/ijsolstr

Using *M*-integral for multi-cracked problems subjected to nonconservative and nonuniform crack surface tractions

J.H. Chang [a,*], W.H. Wu [b]

[a] Department of Civil Engineering, National Central University, Taiwan
[b] Department of Mathematics, National Central University, Taiwan

ARTICLE INFO

Article history:
Received 4 August 2010
Received in revised form 11 April 2011
Available online 25 May 2011

Keywords:
Multiple cracks
Crack surface tractions
M-integral
Path-independence
Surface creation energy

ABSTRACT

In this paper, an energy parameter based on the concept of the *M*-integral is proposed for describing the fracture behavior of a multi-cracked solid subjected to nonconservative and nonuniform crack surface tractions. By using the *M*-integral with a suitably chosen closed contour, one can evaluate the 'surface creation energy' (SCE) required for creation of the stressed cracks. Also, it is demonstrated that the property of path-independence holds even under the action of crack surface tractions. Therefore, the singular stress field in the near-tip areas is not directly involved in the calculation so that a complicated finite element model around the crack tips is not required in evaluation of the *M*-integral.

1. Introduction

For engineering structures containing multiple distributed cracks, the local stress state in the near-tip region becomes quite complicated and difficult to describe. In such a case, the use of energy parameters in describing the 'global' fracture state of the multi-cracked fracture state is therefore of practical interest. The well-known energy conservation contour integrals derived from Noether's theorem in plane elasticity include the J_k-, *M*-, and *L*-integrals (Knowles and Sternberg, 1972; Budiansky and Rice, 1973). Among them, the J_k-integrals ($k = 1,2$) have widely been used as energy fracture parameters for single-cracked problems. Physically, J_k evaluate the energy release rates related to crack extension in quasi-brittle materials. Nevertheless, the J_k-integrals are not suitable for use in characterizing the multi-cracked energy state due to their 'local' nature associated with a single crack tip.

As to the *M*-integral, while not as commonly used as J_k, it has been used in problems containing a single crack (e.g., Herrmann and Herrmann, 1981; Eischen and Herrmann, 1987; Seed, 1997). In these applications, the integration contours were delimited in various ways. Such flexibility implies its applicability to fracture analysis for multi-cracked problems. In the last decade, the *M*-integral has been used for problems containing multiple traction-free cracks for linear elasticity (Chen, 2001; Chen and Lu, 2003, etc.) and hyperelastic materials (Chang and Lin, 2007). An important issue addressed in these works is that, for the condition when the cracks are embedded in an infinite medium and subjected to a uniform far-field loading system, the result of *M* is independent of the coordinate origin. In such a condition, by suitably choosing an integration contour, the *M*-integral evaluates twice the surface creation energy (SCE) associated with creation of all the cracks and can be used as an energy fracture parameter.

In engineering applications, nonconservative and nonuniform tractions along the crack surfaces – which may be due to pressurized fluids, contact pressure, and interfacial friction – are of special interest. In this case, formulation of the energy conservation contour integrals needs to be modified. Discussion on this issue for problems concerning a single crack tip has been presented (Chang and Wu, 2001). Nevertheless, more investigations on multi-cracked problems are still in need.

The objective of this paper is to evaluate the SCE associated with creation of multiple cracks in 2D elastic solids. In addition to the external loading system, the study is considered especially for problems subjected to nonconservative and nonuniform crack surface tractions. An energy parameter based on the concept of the *M*-integral is proposed for this purpose. The integral is shown to be path-independent, even under the action of crack surface tractions. As a consequence, accurate solution can be easily obtained by direct use of numerical schemes such as finite element method. This energy parameter can be used to quantitatively characterize the effect of the crack surface tractions on the mechanical strength of the multi-cracked solids.

* Corresponding author. Tel.: +886 3 4227151; fax: +886 3 4252960.
E-mail address: t320001@cc.ncu.edu.tw (J.H. Chang).

0020-7683/$ - see front matter © 2011 Elsevier Ltd. All rights reserved.
doi:10.1016/j.ijsolstr.2011.05.005

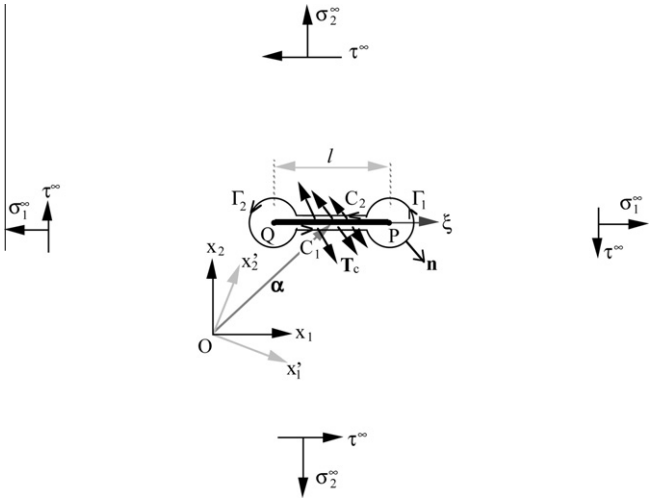

Fig. 1. A 2-D infinite elastic solid, containing a single crack, is subjected to a far-field uniform loading system and nonuniform traction $\mathbf{T}_c$ on the crack surfaces.

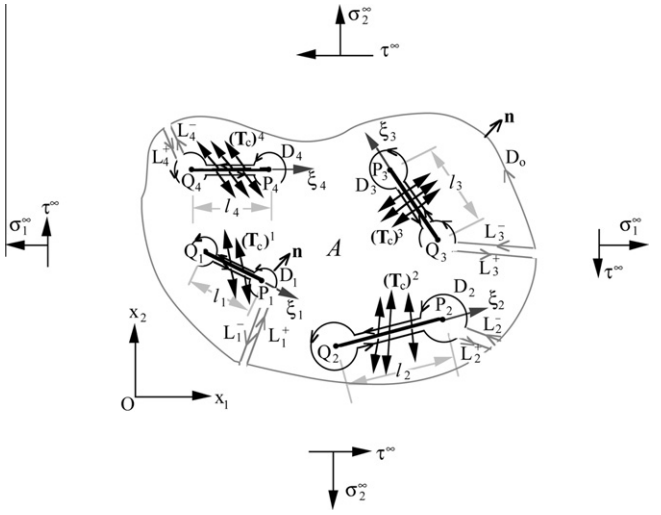

Fig. 2. An infinite elastic solid, containing N distributed cracks ($N = 4$ in this figure), is subjected to a far-field uniform load system and nonuniform tractions on the crack surfaces.

2. The *M*-integral

2.1. A single crack

Consider a 2-D infinite elastic solid, containing a single crack of length l and with two tips P and Q (Fig. 1). A coordinate system originating at an arbitrarily chosen point O is introduced and, with no loss of generality, the crack parallel to the x_1-direction. The position vector at the crack center is denoted as $\boldsymbol{\alpha}$. Under the action of a far-field uniform loading system $(\sigma_1^\infty, \sigma_2^\infty, \tau^\infty)$, the body is homogeneously stressed except in the local neighborhood of the cracked area. In addition, the crack is subjected to nonuniform traction vector $\mathbf{T}_c$ on its surfaces. When the body force is neglected, the M-integral for this crack with respect to O is defined as

$$M = \int_D \left[W n_i x_i - T_j \left(\frac{\partial u_j}{\partial x_i} \right) x_i \right] \mathrm{d}s \tag{1}$$

where D is a counterclockwise closed contour around the whole crack and consists of four parts $C_1 + \Gamma_1 + C_2 + \Gamma_2$, W is the strain energy density of the material, $\mathbf{T}$ is the traction vector, $\mathbf{n}$ is the outward unit vector normal to D, s is the arc length, $\mathbf{x}$ is the position vector of the integration point, and $\mathbf{u}$ is the displacement vector. By definition, the integration is carried out by taking the limiting case where Γ_1 and Γ_2 are shrunk onto the crack tips P and Q, respectively, and C_1 and C_2 are lying along the crack surfaces (this limiting case is not shown in Fig. 1).

It can be shown that M is related to the J_k-integrals as

$$\begin{aligned} M = {} & \alpha_1 \left[\left(J_1^P - J_1^Q \right) - \int_{C_1+C_2} (T_c)_j \frac{\partial u_j}{\partial x_1} \mathrm{d}\xi \right] \\ & + \alpha_2 \left\{ \left(J_2^P - J_2^Q \right) + \int_{C_1+C_2} \left[W n_2 - (T_c)_j \frac{\partial u_j}{\partial x_2} \right] \mathrm{d}\xi \right\} \\ & + \frac{l}{2} \left(J_1^P + J_1^Q \right) - \int_{C_1+C_2} \xi (T_c)_j \frac{\partial u_j}{\partial \xi} \mathrm{d}\xi \end{aligned} \tag{2}$$

where J_k^P and J_k^Q are the J_k-integrals evaluated along Γ_1 and Γ_2, respectively, with J_k^P being defined as

$$J_k^P = \lim_{\Gamma \to 1 \to 0} \int_{\Gamma_1} \left[W n_k - T_j \left(\frac{\partial u_j}{\partial x_k} \right) \right] \mathrm{d}s \quad k = 1, 2 \tag{3}$$

Also, ξ is the local coordinate system originated at the crack center and lying along the crack. Again, by definition, the J_k integrals are evaluated by taking the limiting case in which Γ_1 and Γ_2 are shrunk towards P and Q. Further, it can easily be shown that, while the value of J_k-integrals depends on the orientation of the coordinate system, the quantities in Eq. (2) are independent of the orientation of the coordinate system. Such a characteristic implies that M remains unchanged when the integral is evaluated with respect to an arbitrarily oriented system, e.g., $x_1' - x_2'$ depicted in Fig. 1.

2.2. Multiple cracks

The 2-D infinite elastic solid containing N distributed cracks, each of length l_r ($r = 1, \ldots, N$) and with random location and orientation, as shown in Fig. 2, is homogeneously stressed under a far-field uniform loading system $(\sigma_1^\infty, \sigma_2^\infty, \tau^\infty)$. In addition, the nonuniform traction vector $(\mathbf{T}_c)^r$ is applied on the surfaces of the rth crack. A coordinate system originating at an arbitrarily chosen point O is introduced. When the body force is neglected, the M-integral for all the cracks with respect to O can be defined as

$$M \equiv \sum_{r=1}^{N} \int_{D_r} \left[W n_i x_i - T_j \left(\frac{\partial u_j}{\partial x_i} \right) x_i \right] \mathrm{d}s \tag{4}$$

where D_r is the counterclockwise closed contour associated with the rth crack. Again, by definition, the integration is performed by taking the limiting case in which the portions of D_r are shrunk onto the crack tips and lying along the crack surfaces. Also, while the value of M varies with respect to different selections of origin O, the result of M appears to be invariant with respect to the orientation of the coordinate system.

3. Path-independence

While the property of path-independence for the M-integral has been established for problems containing multiple traction-free cracks (e.g., Chen, 2001). the validity of this property still needs to be investigated when the cracks are subjected to surface tractions.

To this end, we first take an outer contour D_o (Fig. 2) that can be arbitrarily chosen (except for the requirements to be inside the body, enclose all the N cracks, and contain no other singularity in it). Then, by introducing the pairs of cut paths L_r^+ and L_r^- ($r = 1, \ldots, N$), which coincides with each other asymptotically, and delimiting the closed contour $C = (D_r + L_r^+ + L_r^-) - D_o$, we can thus rewrite Eq. (4) as

$$M=\int_C\left[Wn_ix_i-T_j\left(\frac{\partial u_j}{\partial x_i}\right)x_i\right]\mathrm{d}s+\int_{D_o}\left[Wn_ix_i-T_j\left(\frac{\partial u_j}{\partial x_i}\right)x_i\right]\mathrm{d}s \tag{5}$$

Further, we consider the region A enclosed by C, where A is simply-connected due to introduction of the cut paths L_r^+ and L_r^-. By applying divergence theorem in A, we can rewrite the first integration on the right hand side of Eq. (5) as

$$\int_A\left[\left(\frac{\partial W}{\partial x_i}-\sigma_{jm}\frac{\partial u_{j,m}}{\partial x_i}\right)x_i+\left(W\delta_{ii}-\sigma_{jm}\frac{\partial u_j}{\partial x_m}\right)-\frac{\partial\sigma_{jm}}{\partial x_m}\frac{\partial u_j}{\partial x_i}x_i\right]\mathrm{d}a \tag{6}$$

where $\boldsymbol{\sigma}$ is the stress tensor, $\boldsymbol{\delta}$ is the Kronecker delta tensor, and da is the infinitesimal integration area. Note that the first integrand of Eq. (6) vanishes when the material enclosed in A is homogeneous in both the x_1- and x_2-directions. Also, by taking the constitutive relation and the state of equilibrium (with no body force, i.e., $\sigma_{jm,m}=0$), we observe that both the second and third integrands of Eq. (6) vanish.

From Eqs. (5) and (6), the M-integral then reduces to

$$M=\int_{D_o}\left[Wn_ix_i-T_j\left(\frac{\partial u_j}{\partial x_i}\right)x_i\right]\mathrm{d}s \tag{7}$$

Eq. (7) indicates that the M-integral is path-independent, i.e., the integral can be carried out along any outer contour D_o, with the result remaining unchanged. With this property, the integration contour can be more easily defined with no need to accommodate the complex geometry of the set of cracks.

4. Origin-independence

Since the position vector $\mathbf{x}$ is included in the M-integral, the result of this integration thus in general varies with the selection of origin O. In this section, this property will be investigated for the set of N cracks in an infinite body under the action of $(\sigma_1^\infty,\sigma_2^\infty,\tau^\infty)$ and $(\mathbf{T}_c)^r$ ($r=1,\ldots,N$, as shown in Fig. 2).

By substituting Eqs. (1) and (2) into Eq. (4), the M-integral for the N cracks with respect to O can be expressed as

$$\begin{aligned}M=\sum_{r=1}^{N}\Bigg\{&\alpha_1^r\left[\left(J_1^{\mathrm{Pr}}-J_1^{\mathrm{Qr}}\right)-\int_{C_1^r+C_2^r}(T_c)_j^r\frac{\partial u_j}{\partial x_1}\mathrm{d}\xi^r\right]\\&+\alpha_2^r\left\{\left(J_2^{\mathrm{Pr}}-J_2^{\mathrm{Qr}}\right)+\int_{C_1^r+C_2^r}\left[Wn_2^r-(T_c)_j^r\frac{\partial u_j}{\partial x_2}\right]\mathrm{d}\xi^r\right\}\\&+\frac{l_r}{2}\left(J_1^{\mathrm{Pr}}J_1^{\mathrm{Qr}}\right)-\int_{C_1+C_2}\xi^r(T_c)_j^r\frac{\partial u_j}{\partial\xi^r}\mathrm{d}\xi^r\Bigg\}\end{aligned} \tag{8}$$

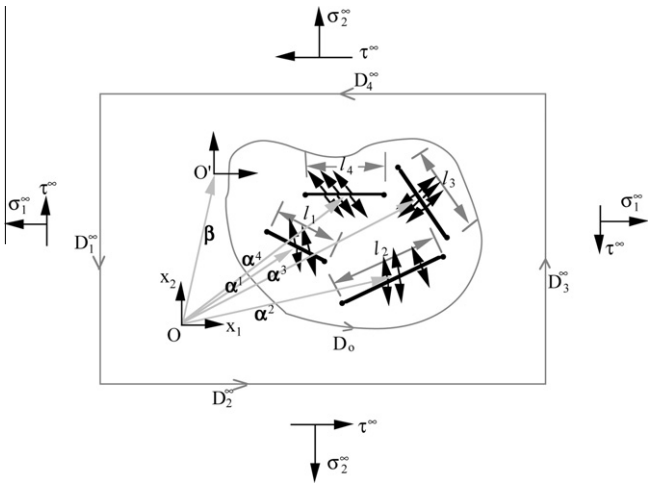

Fig. 3. A remote rectangular contour D^∞ is chosen for this integration.

where $\boldsymbol{\alpha}^r$ is the position vector of the rth crack center with respect to O (as shown in Fig. 3), J_k^{Pr} and J_k^{Qr} are the J_k-integrals associated with the tips P_r and Q_r, respectively, C_1^r and C_2^r are the line segments along the rth crack surfaces, ξ^r is the local coordinate system originated at the rth crack center, and n_2^r is the outward unit vector normal to $C_1^r+C_2^r$.

Due to path-independence, the integration can be carried out along any arbitrarily chosen closed contour D_o that encloses all the N cracks, with the value remaining unchanged. Here, a remote rectangular contour $D^\infty(=D_1^\infty+D_2^\infty+D_3^\infty+D_4^\infty)$ is chosen. Also, by taking another arbitrarily chosen point O' as the reference point, we can rewrite Eq. (8) as

$$\begin{aligned}M=&\Bigg\{\sum_{r=1}^{N}(\alpha_1^r-\beta_1)\left[\left(J_1^{\mathrm{Pr}}-J_1^{\mathrm{Qr}}\right)-\int_{C_1^r+C_2^r}(T_c)_j^r\frac{\partial u_j}{\partial x_1}\mathrm{d}\xi^r\right]\\&+(\alpha_2^r-\beta_2)\left[\left(J_2^{\mathrm{Pr}}-J_2^{\mathrm{Qr}}\right)+\int_{C_1^r+C_2^r}\left[Wn_2^r-(T_c)_j^r\frac{\partial u_j}{\partial x_2}\right]\mathrm{d}\xi^r\right]\Bigg\}\\&+\left[\sum_{r=1}^{N}\frac{l_r}{2}\left(J_1^{\mathrm{Pr}}J_1^{\mathrm{Qr}}\right)-\int_{C_1+C_2}\xi^r(T_c)_j^r\frac{\partial u_j}{\partial\xi^r}\mathrm{d}\xi^r\right]\\&+\beta_k\int_{D^\infty}\left[Wn_k-T_j\left(\frac{\partial u_j}{\partial x_k}\right)\right]\mathrm{d}s\end{aligned} \tag{9}$$

where $\boldsymbol{\beta}$ is the position vector of O'. Note that, since D^∞ is chosen to be far from the cracked region, the stresses and the strain energy density W are thus homogeneous along the contour. Also, the spatial derivatives of the far-field displacements are also uniform. Therefore, the last term of Eq. (9) (i.e., the integration along D^∞) intrinsically vanishes for both $k=1$ and 2 in that all the state variables are homogeneously distributed. This indicates that the M-integral in Eq. (9), which is originally defined with respect to the origin O, appears to be equivalent to that evaluated with respect to another point O'. This means that the location-dependent terms in both equations are equal to each other and actually vanish since O' can be arbitrarily chosen. Thus, both equations reduce to the following origin-independent expression as

$$M=\sum_{r=1}^{N}\left[\frac{l_r}{2}\left(J_1^{\mathrm{Pr}}+J_1^{\mathrm{Qr}}\right)-\int_{C_1+C_2}\xi^r(T_c)_j^r\frac{\partial u_j}{\partial\xi^r}\mathrm{d}\xi^r\right] \tag{10}$$

Eq. (10) indicates that, for a homogeneously-stressed infinite solid under the action of nonuniform crack surface tractions, the M-integral is origin-independent.

As an aside, it is noted that the last term of Eq. (9) actually corresponds to the integration of J_k. Due to path-independence, the integration can be carried out along D^∞ or any arbitrarily chosen closed contour that encloses all the N cracks, The vanishing feature indicates that the J_k-integrals are not suitable for use in characterizing the multi-cracked energy state.

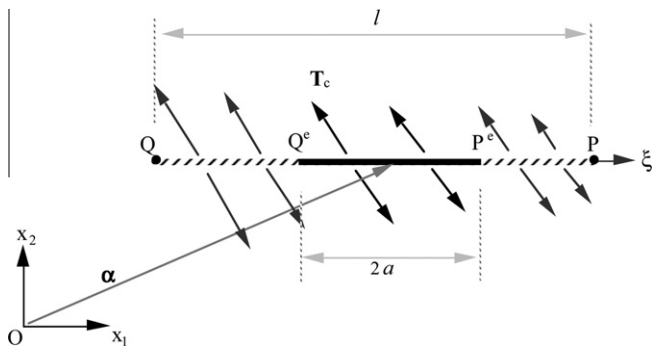

Fig. 4. An intermediate state for the crack during its evolution. The crack is subjected to nonconservative and nonuniform surface tractions.

5. Physical interpretation

In this section, the physical meaning of the M-integral is to be illustrated. By considering a single crack with two tips P and Q and of length l, we arbitrarily choose an intermediate state during the process of its self-expansion, as shown in Fig. 4. At this stage, the crack is of length $2a$ and instantly terminated at, say, point P^e and point Q^e. Note that, the surface traction $\mathbf{T}_c$ is not present until the crack surfaces are created due to its nonconservative nature. In Fig. 4, the portion of the crack that remains to be formed and the corresponding to-be-present surface tractions are depicted in dashed lines. The associated energy release rate G, due to a unit advance at the point P^e along the original direction of the crack segment, can be expressed as decrease of the potential energy Π and related to the coordinate component ξ as

$$G = -\frac{\mathrm{d}\Pi}{\mathrm{d}a} = -\frac{\mathrm{d}\Pi}{\mathrm{d}\xi}\frac{\mathrm{d}\xi}{\mathrm{d}a} \tag{11}$$

and

$$\xi = a \text{ for } \xi \geqslant 0, \text{ and } \xi = -a \text{ for } \xi < 0 \tag{12}$$

The potential energy Π consists of the strain energy and the work done by the far-field loading system. The value of G, as a function of a, is equal to J_1^P and $-J_1^Q$ at tip P and Q, respectively as

$$G|_{\xi=l/2} = -\left.\frac{\mathrm{d}\Pi}{\mathrm{d}a}\right|_{\xi=l/2} = J_1^P \tag{13.1}$$

$$G|_{\xi=-l/2} = -\left.\frac{\mathrm{d}\Pi}{\mathrm{d}a}\right|_{\xi=-l/2} = -J_1^Q \tag{13.2}$$

For an infinite medium subjected to a far-field uniform loading system $\boldsymbol{\sigma}^\infty$, it is observed that G appears to be directly proportional to the (half-) crack length a (e.g., Rivlin and Thomas, 1983; Broek, 1986, etc.). Such linearity also holds under the action of crack surface tractions, as illustrated in Appendix A. In this sense, G can be written in terms of the following separable form

$$G = \Phi a \tag{14}$$

where Φ is a function of the loading conditions and the material parameters.

With the far-field uniform loads remaining unchanged, integration of Eq. (14) throughout the process of crack evolution (by considering Eqs. (13.1) and (13.2)) yields

$$\Delta\Pi = -\int_{\xi=-l/2}^{\xi=l/2} G\,\mathrm{d}a = -\frac{1}{2}\Phi a^2\Big|_{\xi=-l/2}^{\xi=l/2} = -\frac{1}{2}\left[\frac{l}{2}\left(J_1^P + J_1^Q\right)\right] \tag{15}$$

By substituting Eq. (15) into Eq. (10) (with $N = 1$), we then have

$$M = -2(\Delta\Pi + \Delta\mathrm{Wnonc}) = -2\mathrm{SCE} \tag{16}$$

where ΔWnonc is the work done by the nonconservative crack surface tractions and defined as

$$\Delta\mathrm{Wnonc} = \frac{1}{2}\int_{C_1+C_2} \xi(T_c)_j \frac{\partial u_j}{\partial \xi}\mathrm{d}\xi \tag{17}$$

Eq. (16) indicates that the M-integral evaluates twice the SCE (i.e., the sum of the potential energy and nonconservative work) required for creation of the stressed crack. Also, the physical interpretation of the M-integral can be straightforwardly extended to multi-cracked condition in that, as shown by Eq. (4), the result of M can be taken as the summation of those evaluated by each single crack.

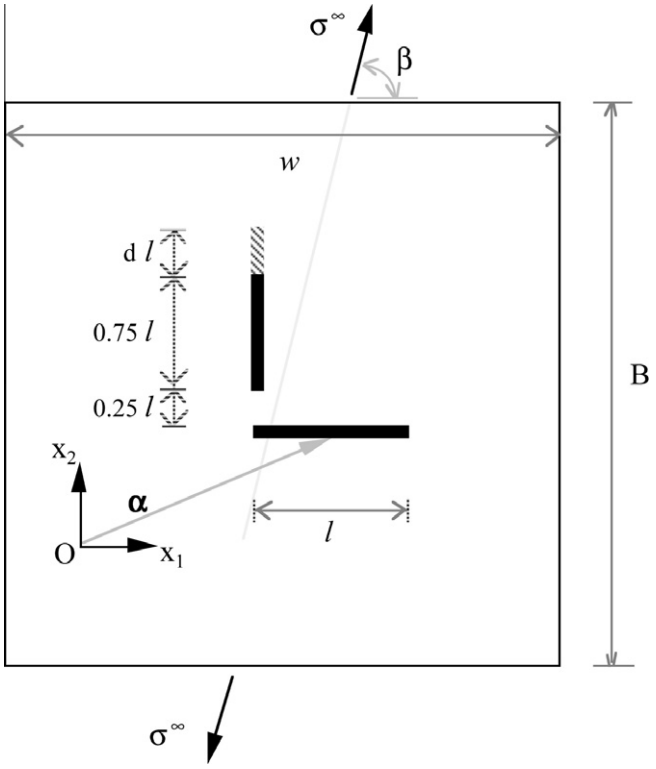

Fig. 5. A plane strain specimen containing two perpendicular cracks.

6. Numerical examples

6.1. Problem 1 (verification)

The aim of this problem is to verify the feasibility of our formulation. To this end, we consider a plane strain isotropic elastic specimen containing two perpendicular cracks of length l and $0.75l$, separated by a distance $0.25l$ from each other, as shown in Fig. 5

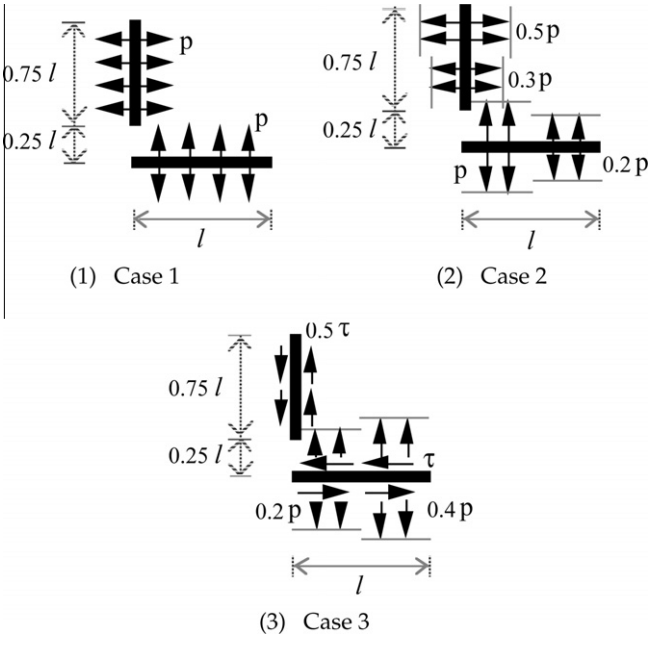

Fig. 6. Three instances of different distributed crack surface tractions.

($E = 30$ MPa and $\nu = 0.25$). The crack length l is relatively small compared with the width w and length B so that the finite width effect of the specimen can be neglected. The specimen is subjected to an oblique uniaxial tensile stress σ^{∞} along the exterior boundaries. Three instances of different distributed crack surface tractions, as shown in Fig. 6, are considered.

The study in this example problem is organized as follows. First, the effect of the local finite element modeling around the crack tips is investigated. Next, the property of path-independence is demonstrated. Subsequently, the origin-independent property of M is examined. Finally, the physical interpretation of M is verified by comparing the result of the integral with the energy change associated with both perturbation of the crack length and creation of the cracks.

For accuracy, it is required that the M-integral be computed with a high degree of precision. To investigate the effect of finite element modeling around the crack tips, two finite element models with very different near-tip local meshes are used to simulate the specimen. In the calculations, quadratic finite elements are used for interpolation of the displacement field. The local portions in the near-tip area for the two FE meshes are shown in Fig. 7. Note that the concept of multi-point constraint is used to tie the fine and coarse elements in the second mesh (Fig. 7(2)) so that continuity of displacement is ensured. Also, no particular singular elements are used. The integration paths are chosen to be far from the crack tips. The results of M, for load case 1, from the two meshes are tabulated in Table 1. Although the mesh around the crack tips in the second model is quite coarse, the results from the two models show very good consistency, with deviation less than 1%. As indicated, the above calculation appears to be rather insensitive to the local mesh in that the near-tip finite element solutions are not directly used when the integration paths are chosen to be far from the crack tips.

Table 1
The results of M from two FE models for problem 1 (Pa m^2).

Mesh 1 (Fig 7(1))	Mesh 2 (Fig 7(2))
2.936	2.954

Note: $w = 150$ cm, $B = 150$ cm, $l = 12$ cm, $\sigma^{\infty} = 40$ kPa, $\beta = 30°$, $p = 100$ kPa, $\boldsymbol{\alpha} = (15,5)$ cm, load case 1.

Three integration paths (as shown in Fig. 8), each enclosing different portion of the same finite element mesh, are used in order to verify path-independence of the calculation. The results with respect to $\boldsymbol{\alpha} = (15,15)$ cm are shown in Table 2. The results obtained from the three contours show very good agreement and the property of path-independence is evident.

In order to show the property of origin-independence, three coordinate systems located at different origins are selected. The values of M with respect to the three choices of $\boldsymbol{\alpha}$ are shown in Table 3. The numerical results indicate that, even when the origin is chosen to be far away from the cracks, deviations of M are observed to be under 1%. The validity of this property is thus verified.

To illustrate the physical meaning of the M-integral, we first consider the same specimen and define another problem with slightly altered crack configuration, where one of the crack tips is extended by a relatively small amount of dl (Fig. 5). Numerically, this is established by perturbing nodal point positions at the crack

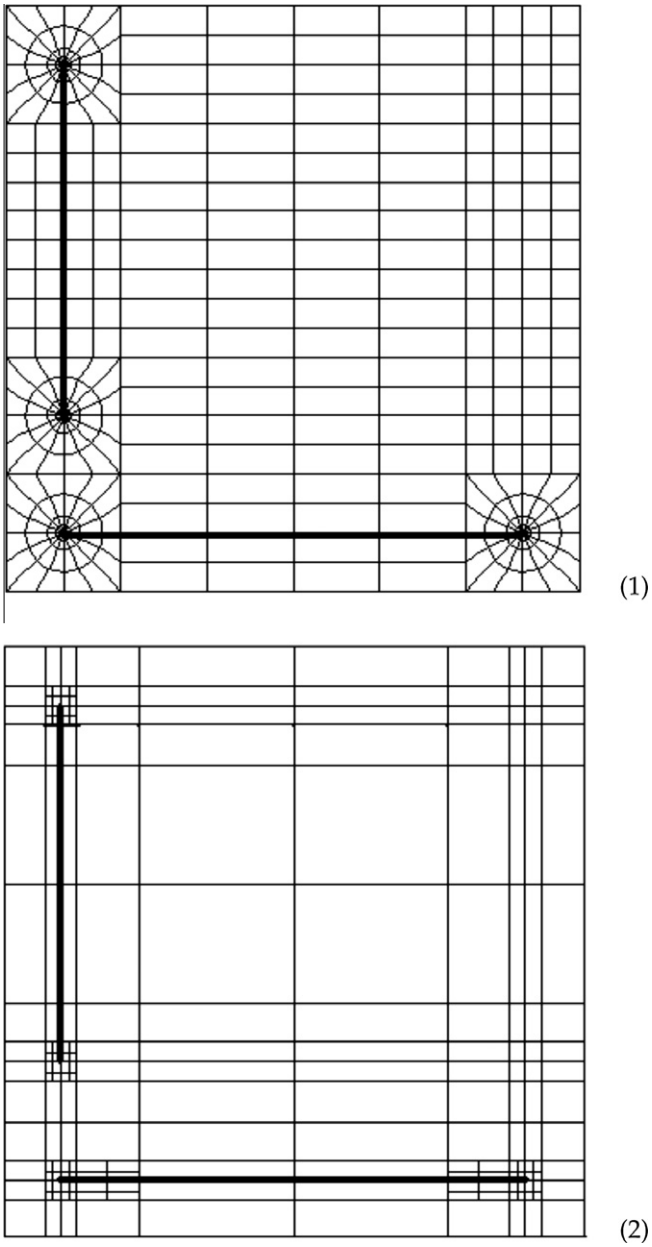

Fig. 7. The local portions in the near-tip area for the two FE meshes.

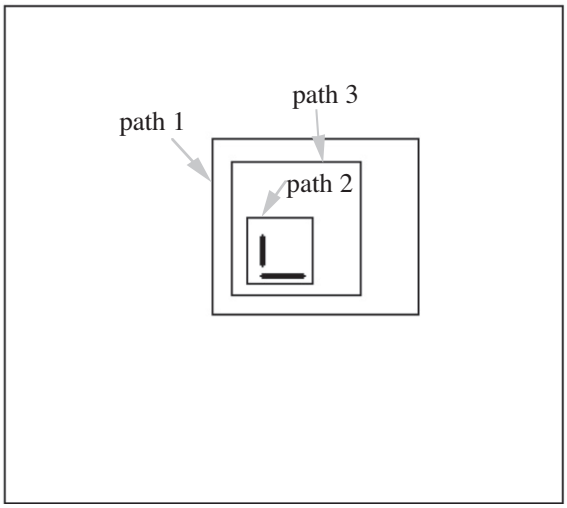

Fig. 8. Three contours are used for the M-integral.

Table 2
The results of M from three integration paths for problem 1 (Pa m^2).

	Path 1	Path 2	Path 3
Case 1 (Fig 6(1))	2.941	2.914	2.936
Case 2 (Fig 6(2))	1.859	1.868	1.855
Case 3 (Fig 6(3))	1.568	1.560	1.553

Note: $w = 150$ cm, $B = 150$ cm, $l = 12$ cm, $\sigma^{\infty} = 40$ kPa, $\beta = 30°$, $p = \tau = 100$ kPa, $\boldsymbol{\alpha} = (15,15)$ cm.

Table 3
The results of M versus different $\boldsymbol{\alpha}$'s for problem 1 (Pa m^2).

$\boldsymbol{\alpha}$	(15,15) cm	(0,0) cm	(100,0) cm
Case 1 (Fig 6(1))	2.936	2.935	2.931
Case 2 (Fig 6(2))	1.859	1.854	1.851
Case 3 (Fig 6(3))	1.568	1.552	1.555

Note: $w = 150$ cm, $B = 150$ cm, $l = 12$ cm, $\sigma^{\infty} = 40$ kPa, $\beta = 30°$, $p = \tau = 100$ kPa.

tip of a given finite element mesh ahead by dl. The mechanical energy, which consists of the potential energy P and the nonconservative work Wnonc, for both the original and the perturbed configurations are then calculated by using finite elements. By evaluating the corresponding energy differences, the values of $-$d($\Delta\Pi$ + ΔWnonc) associated with two selected values of dl, (for load case 1) are listed in Table 4. Also listed in the table are the values of dM, i.e., the variation of M due to the crack growth of dl. Next, we consider the same specimen and take its uncracked state as a reference configuration. Still, the values of the mechanical energy associated with both the cracked and uncracked configurations are calculated by using finite elements. The result of $-(\Delta\Pi + \Delta\text{Wnonc})$, which corresponds to the SCE due to creation of the cracks, is listed in Table 5. Also listed in the table is the FE result of the corresponding M-integral. By comparing the values of both pairs, i.e., $-$d($\Delta\Pi$ + ΔWnonc) and dM/2, $-(\Delta\Pi + \Delta\text{Wnonc})$ and $M/2$, the validity of the physical meaning of M as associated with twice the SCE is thus well demonstrated.

As an aside, it was previously described that the J_k-integrals are not suitable for use in characterizing the multi-cracked energy state due to their vanishing feature. To illustrate this, the first integration path in Fig. 8 is used to evaluate J_k. and the results for the three loading cases are shown in Table 6. By comparing with the values of the M-integral, it is observed that the results of J_k appear to be vanishingly small, as anticipated.

6.2. Problem 2 (application)

In this example, we consider a plane stress isotropic specimen of width w and length B(E = 3 kPa and ν = 0.25). The specimen contains a family of parallel one-sized and pressurized cracks, as shown in Fig. 9. These cracks, each of length l and subjected to nonuniform pressure $p(x_2)$, are distributed in a doubly periodic manner, where s and d denote the spacings of neighboring cracks in

Table 4
Energy released due to perturbed crack length in problem 1 (10^{-3} Pa m^2).

dl/l	$-$d($\Delta\Pi$)	d(ΔWnonc)	$-$d($\Delta\Pi$ + ΔWnonc)	dM/2
0.01/12	7.906	5.845	2.061	2.108
0.02/12	15.818	11.694	4.124	4.218

Note: $w = 150$ cm, $B = 150$ cm, $l = 12$ cm, $\sigma^{\infty} = 40$ kPa, $\beta = 30°$, $p = 100$ kPa, load case 1.

Table 5
Energy change due to creation of the cracks in problem 1 (Pa m^2).

$-\Delta\Pi$	ΔWnonc	$-(\Delta\Pi + \Delta\text{Wnonc})$	$M/2$
7.988	6.534	1.454	1.468

Note: $w = 150$ cm, $B = 150$ cm, $l = 12$ cm, $\sigma^{\infty} = 40$ kPa, $\beta = 30°$, $p = 100$ kPa, load case 1.

Table 6
The results of J_k for problem 1 (Pa m^2).

	J_1	J_2
Case 1 (Fig 6(1))	3.500×10^{-4}	-3.128×10^{-4}
Case 2 (Fig 6(2))	2.427×10^{-4}	-1.852×10^{-4}
Case 3 (Fig 6(3))	1.953×10^{-4}	-0.741×10^{-4}

Note: $w = 150$ cm, $B = 150$ cm, $l = 12$ cm, $\sigma^{\infty} = 40$ kPa, $\beta = 30°$, $p = \tau = 100$ kPa.

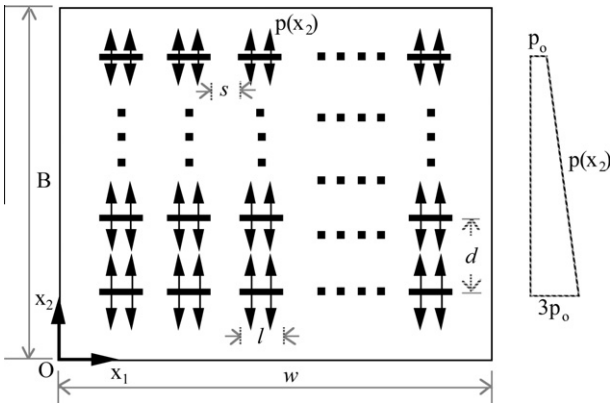

Fig. 9. A plane stress specimen containing a family of parallel pressurized cracks. The pressure $p(x_2)$ varies linearly from p_o to $3p_o$ along the x_2-direction (problem 2).

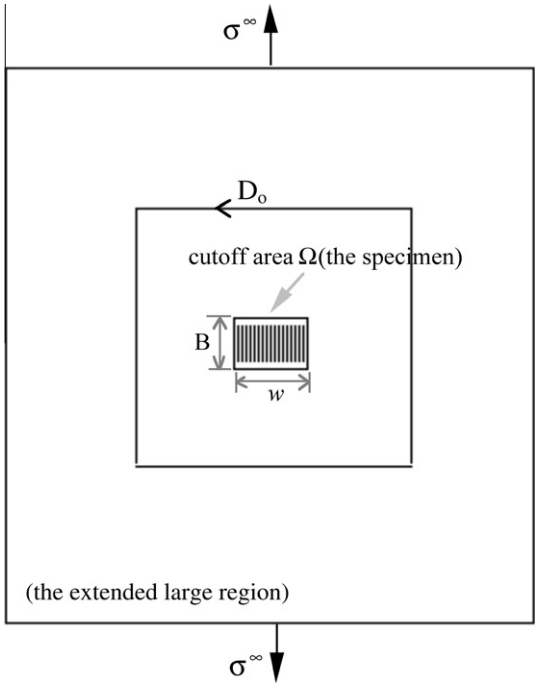

Fig. 10. A cutoff area Ω, which is the specimen in Fig. 9, and an integration path D_o in an extended region (problem 2).

the parallel (x_1-) and perpendicular (x_2-) directions. The magnitude of $p(x_2)$ varies linearly from p_o to $3p_o$ along the x_2-direction.

We further delimit the specimen as a cutoff area Ω in an extended region that is large enough to be regarded as an infinite medium, as shown in Fig. 10. By using an integration path D_o that is far from the crack tips, the M-integral is evaluated with finite elements. Note that it is not necessary to have very fine finite element grids in the near-tip areas in that they are not directly used in evaluating the integral. The crack density can be measured by the crack density parameter f as

$$f = \frac{Nl^2}{4A_\Omega} \tag{18}$$

where N is the total number of cracks, and A_Ω is the area of Ω. Note that the concept of cutoff area is commonly used in the context of micromechanics (e.g., Ju and Chen, 1994; Tsukrov and Novak, 2004, etc). In the following calculations, the area A_Ω and the spacing d are fixed, while the crack length l and the spacing s are varying. With this, five different values of crack density parameter are considered, i.e., f equal to 0.15, 0.24, 0.34, 0.47, and 0.61, respectively.

By applying uniaxial far-field tensile stress σ^∞ in the x_2-direction along the upper and lower boundaries of the extended region (Fig. 10), the M-integral corresponding to various levels of applied pressure $p(x_2)$ is then evaluated. Although not shown in detail here, the results appear to be independent of both the integration path and the origin. The results of M, associated with the five values of f, are depicted versus the loading ratio p_o/σ^∞ and shown in Fig. 11. As can be seen from the figure, the value of M at a fixed crack density appears to be nearly proportional to the level of the applied pressure p_o. More discussions on such a feature are presented in Appendix B. Also, the results indicate that M is a monotonically increasing function of the crack density.

The above results indicate that the M-integral essentially characterizes the effect due to different crack density and pressurized conditions. Application of M would then facilitate understanding of the degradation of materials induced by the crack surface traction and furnish the associated information needed to describe the damage state. Therefore, by using the results of M, the influence due to $p(x_2)$ can be effectively quantified. A 'pressurized index' (PI), for example, can be defined for this purpose. To this end, by considering a fixed f and taking the unpressurized state as a reference, the value of M at this reference state is denoted as $M_{\text{ref},f}$. The result of M under the action of $p(x_2)$ is then normalized with respect to $M_{\text{ref},f}$, and the pressurized index can be defined as

$$PI = \frac{M}{M_{\text{ref},f}} - 1 \tag{19}$$

Physically, PI measures the increment of normalized SCE induced by $p(x_2)$ from its unpressurized reference state.

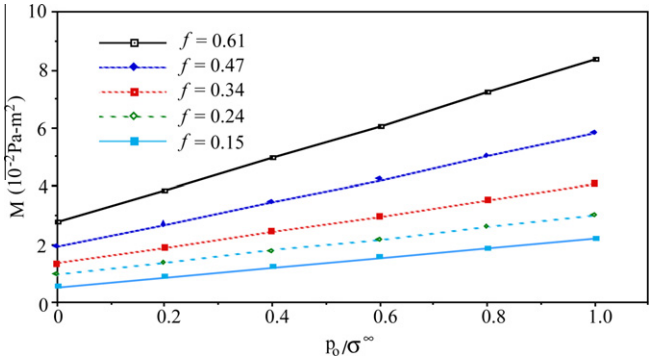

Fig. 11. The values of M versus the loading ratio p_o/σ^∞ (problem 2). (Note: w = 150 cm, B = 150 cm, d = 0.25 cm, σ^∞ = 10 kPa).

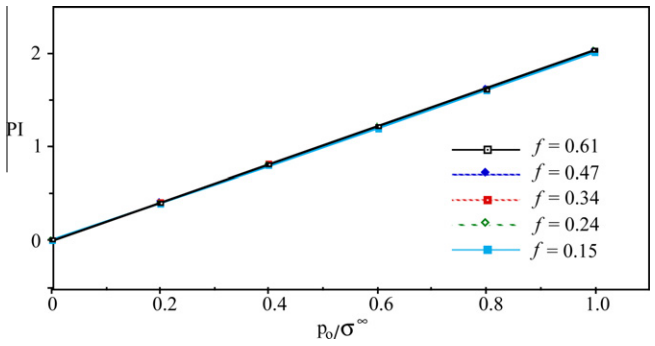

Fig. 12. The pressurized index versus the loading ratio p_o/σ^∞ (problem 2). (Note: w = 150 cm, B = 150 cm, d = 0.25 cm, σ^∞ = 10 kPa.)

The results of PI versus the loading ratio p_o/σ^∞, under five different values of f. are shown in Fig. 12. As can be seen from the figure, the values of PI appear to vary proportionally with p_o/σ^∞ at a fixed f. The increase in p_o/σ^∞ from 0 to 1 raises the value of PI from 0 to, approximately, 2. It is also observed that the five curves bear almost indistinguishable trend, i.e., there is almost no variation of PI with f. The results indicate that, at a fixed crack density, the SCE corresponding to creation of the crack system increases by twice as the value of p_o/σ^∞ increases up 1. Such an effect appears to be very similar for different values of f for the problem considered in this example.

We further take the applied far-field stresses, along with the corresponding averaged strain components of the specimen, and define their ratios as the 'stiffness index' tensor **SI** for the specimen. For example, for the far-field stress σ^∞ in Fig. 10, the component SI_{22} for Ω is defined as

$$SI_{22} = \frac{\sigma^\infty}{\left[\frac{\int_0^B \int_0^w \varepsilon_{22}(x_1,x_2)\,dx1\,dx2}{Bw}\right]} \tag{20}$$

where $\varepsilon_{22}(x_1,x_2)$ is the normal strain component in the x_2-direction. For pressurized cracks under fixed value of σ^∞, $\varepsilon_{22}(x_1,x_2)$ in Ω appears to increase as the pressurized level increases. Such 'softening' behavior induced by presence of the 'internal' pressure can thus be properly characterized by the decrease of SI_{22}. In addition to directly evaluate the SCE, the result of M can also be used to evaluate the change of **SI** under the action of the nonuniform pressure $p(x_2)$. To this end, we have the correspondence relation between **SI** of Ω and the SCE associated with creation of these cracks expressed (Shen and Li, 2004) as

$$\boldsymbol{\sigma}^\infty : [(\mathbf{SI} - \mathbf{H})^{-1} : \mathbf{H} + \mathbf{S}]^{-1} : \mathbf{H}^{-1} : \boldsymbol{\sigma}^\infty = -2SCE/A_\Omega \tag{21}$$

where **H** is the elastic stiffness tensor of the matrix material, **S** is the Eshelby tensor. By substituting the above solutions of M into Eqs. (16) and (21), **SI** can then be evaluated.

The feasibility of using M-integral for evaluating **SI** can be demonstrated by considering the special condition when the cracks are unpressurized (i.e., $p_o/\sigma^\infty = 0$). In such a case, **SI** is equal to the effective stiffness that is commonly used in micromechanics for describing the decrease of material integrity due to evolution of cracks. The results of the normalized SI_{22}, which is equal to the normalized effective Young's modulus E_{22}/E, versus the crack density parameter are shown in Fig. 13. Also included in the figure are the solutions from other two approaches (Nemat-Nasser et al., 1993; Shen and Li, 2004). As can be seen, our results by using M are in good agreement with those from these two methods. Also, when compared with other existing methods, our presented formulation appears to be more straightforward in practice since the effective stiffness is determined by using a scalar parameter

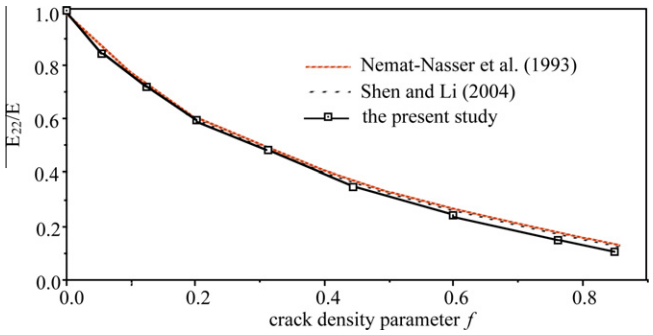

Fig. 13. The normalized effective elastic moduli E_{22}/E (=SI_{22}/E) for Ω versus the crack density parameter (problem 2, $p_o/\sigma^\infty = 0$).

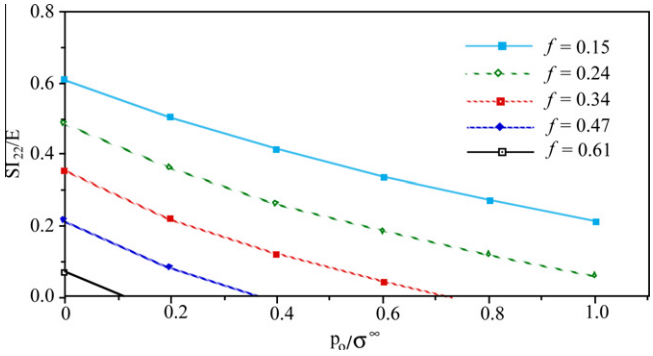

Fig. 14. The normalized SI_{22}/E for Ω versus the loading ratio p_o/σ^∞ (problem 2). (Note: w = 150 cm, B = 150 cm, d = 0.25 cm, σ^∞ = 10 kPa.)

(i.e., M) rather than the conventionally-used algebraic matrix systems.

The influence due to the pressurized level on the normalized stiffness index is illustrated in Fig. 14, where the results of SI_{22}/E for the five values of f, are depicted versus the loading ratio p_o/σ^∞. Again, all the curves bear very similar trend with respect to p_o/σ^∞. Also, it is seen that the value of SI_{22} drops and even vanishes as the value of f and p_o/σ^∞ increases. This indicates that, for certain values of f and p_o/σ^∞, the averaged value of the tensile strain $\varepsilon_{22}(x_1,x_2)$ in Ω becomes so large that SI_{22}/E may even reaches zero.

The concept of **SI** can be used as an efficient tool in practical applications. For example, for an underground damaged structure, the crack surfaces are subjected to groundwater pressure whose magnitude may change spatially due to variations in depth, groundwater level, and drainage condition, etc. A numerical analysis by using, say, finite elements is hereby conducted for evaluation of the deformed state caused by the crack surface pressures and other applied loads. Nevertheless, in order to explicitly apply the crack surface pressure as a specified boundary condition, each individual crack needs to be properly modeled in the finite element model. This is not applicable in practice especially for the condition when there can be more than hundreds and thousands of cracks in the structure. Alternatively, with the concept of **SI**, the influence from the magnitude of pressure level can be treated implicitly in the same manner as that used for treatment of the distributed multiple cracks in micromechanics. In this sense, both the crack density parameter f and the normalized pressure level p/p_{ref} (where p_{ref} is an arbitrarily chosen reference pressure level) are regarded as mechanical factors that affect the stiffness of the corresponding material and/or structure and can then be easily implemented for subsequent analyzes. Based on this consideration, the damage phenomena which covers combinations of f and p/p_{ref} for structures containing multiple pressurized cracks can thus be effectively simulated, accurately quantified, and straightforwardly built in for further computation.

7. Conclusion

The M-integral is generally origin-dependent. Nevertheless, for an infinite medium containing multiple traction-free cracks under a uniform far-field loading system, it has been well acknowledged that the value of M-integral is independent of the coordinate origin, In this paper, it is further illustrated that the origin-independent property holds when the cracks are subjected to nonuniformly distributed surface tractions.

Physically, the M-integral evaluates (twice) the SCE corresponding to creation of the stressed cracks. Also, due to path-independence, the integration contour can be arbitrarily chosen as long as they contain the whole set of cracks. Hence, the complicated singular stress field in the near-tip areas is not directly involved in the calculation. Based on this characteristic, it is therefore suggested that M be practically used as an energy parameter for describing the decrease of material integrity of the multi-cracked solids under the action of nonconservative and nonuniform crack surface tractions.

Acknowledgments

This work has been partially supported by National Science Council Grant No. NSC98-2221-E-008-071 to National Central University.

Appendix A

In order to investigate the effect of the crack length under the action of crack surface tractions, we consider a single crack subjected to a far-field uniform loading system, e.g., $(\sigma_1^\infty, \sigma_2^\infty, \tau^\infty) = (0, 4\sigma, \sigma)$ and different nonuniform pressures on the crack surfaces. The values of G at tip P with respect to varying crack length, under three loading conditions in plane strain, are evaluated by calculating the associated J_1-integral with finite elements here. The results are sketched in Fig. A.1. The validity of this linear relation between G and l is thus evident.

Appendix B

We consider a single crack subjected to uniaxial far-field tensile stress σ^∞ in the x_2-direction and uniform pressure p_o on the crack

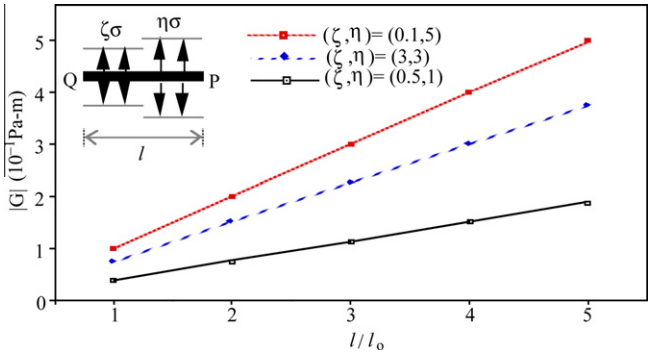

Fig. A.1. The results of G vs l under three loading conditions on the crack surfaces. (Note: l_o = 3 cm, σ = 100 kPa.)

surfaces. For plane stress, the result of $\Delta\Pi$ due to creation of the pressurized crack (Eq. (15)) can analytically be expressed as

$$\Delta\Pi = -\frac{1}{2}\left[\frac{l}{2}\left(J_1^P + J_1^Q\right)\right] = -\frac{1}{4E} - \pi(p_o + \sigma^\infty)^2 l^2 \tag{A.1}$$

As an aside, by combined use of analytical asymptotic approach (in the near-tip region) and finite element method (in the nonsingular area), the integration for ΔWnonc in Eq. (17) can be evaluated and written as

$$\Delta\text{Wnonc} = \frac{1}{2}\int_{C_1+C_2} \xi(T_c)_j \frac{\partial u_j}{\partial \xi} \mathrm{d}\xi = 0.787\frac{1}{E}(p_o^2 + \sigma^\infty p_o) l^2 \tag{A.2}$$

Then, substituting Eq. (A.1) and (A.2) into Eq. (16) results in

$$M = \frac{1}{2E}\pi(\sigma^\infty)^2\left[-0.002\left(\frac{p_o}{\sigma^\infty}\right)^2 + 0.998\left(\frac{p_o}{\sigma^\infty}\right) + 1\right] l^2 \tag{A.3}$$

As illustrated in Eqs. (A.1)–(A.3), while $\Delta\Pi$ and ΔWnonc are both characterized by quadratic function of p_o, this leading quadratic term for M is almost eliminated and makes rather insignificant contribution when their summation is taken. The value of M is thus governed by the linear term of p_o. Such a feature appears to be more significant when $p_o/\sigma^\infty < 1$.

References

Broek, D., 1986. Elementary Engineering Fracture Mechanics, fouth ed. Martinus Nijhoff Publishers.

Budiansky, B., Rice, J.R., 1973. Conservation laws and energy-release rates. J. Appl. Mech. 40, 201–203.

Chang, J.H., Lin, J.S., 2007. Surface energy for creation of multiple curved cracks in rubbery materials. J. Appl. Mech. 74, 488–496.

Chang, J.H., Wu, W.H., 2001. FE calculation of contour integrals in plane anisotropic elastic media with crack surface tractions. Fin. Elem. Anal. Des. 37, 673–686.

Chen, Y.H., 2001. *M*-integral analysis for two-dimensional solids with strongly interacting microcracks. Part I: in an infinite brittle solid. Int. J. Solids Struct. 38, 3193–3212.

Chen, Y.H., Lu, T.J., 2003. Recent developments and applications of invariant integrals. Appl. Mech. Rev. 56, 515–552.

Eischen, J.W., Herrmann, G., 1987. Energy release rates and related balance laws in linear elastic defect mechanics. J. Appl. Mech. 54, 388–392.

Herrmann, A.G., Herrmann, G., 1981. On energy release rates for a plane crack. J. Appl. Mech. 48, 525–528.

Ju, J.W., Chen, T.M., 1994. Micromechanics and effective moduli of elastic composites containing randomly dispersed ellipsoidal inhomogeneities. Acta Mech. 103, 103–121.

Knowles, J.K., Sternberg, E., 1972. On a class of conservation laws in linearized and finite elastostatics. Arch. Rat. Mech. Anal. 44, 187–211.

Nemat-Nasser, S., Yu, S., Hori, M., 1993. Solids with periodically distributed cracks. Int. J. Sol. Struct. 30, 2071–2095.

Rivlin, R.S., Thomas, A.G., 1983. The incipient characteristic tearing energy for an elastomer crosslinked under strain. J. Poly. Sci. Poly. Phys. 21, 1807–1814.

Seed, G.M., 1997. The Boussinesq wedge and the J_k, L, and M integrals. Fatigue Fract. Eng. Mater. Struct. 20 (6), 907–916.

Shen, L., Li, J., 2004. A numerical simulation for effective elastic moduli of plates with various distributions and sizes of cracks. Int. J. Solids Struct. 41, 7471–7492.

Tsukrov, I., Novak, J., 2004. Effective elastic properties of solids with two-dimensional inclusions of irregular shapes. Int. J. Solids Struct. 41, 6905–6924.